Desalination and Water Treatment
www.deswater.com
doi: 10.5004/dwt.2019.23701

147 (2019) 243–254
April

Modification of bentonite by Al/Mg-polymeric hydroxy for Cu^{2+}, Cd^{2+}, and Pb^{2+} removal from aqueous solutions

Liheng Liu[a,b,c], Chuanwu Tang[a,b,c], Yali Peng[a,b,c], Fei Pan[a,b,c], Hua Lin[a,b,c,*], Xuehong Zhang[a,b,c,*], Kong Chhuon[d]

[a]*College of Environmental Science and Engineering, Guilin University of Technology, Guilin 541004, China, Tel./Fax: +86 (773) 2536922; emails: linhua5894@163.com (H. Lin), zhangxuehong@x263.net (X. Zhang), deanhenry_liu01@126.com (L. Liu), 813702685@qq.com (C. Tang), 1158499438@qq.com (Y. Peng), 361281014@qq.com (F. Pan)*
[b]*Guangxi Key Laboratory of Environmental Pollution Control Theory and Technology, Guilin University of Technology, Guilin 541004, China*
[c]*Collaborative Innovation Center for Water Pollution Control and Water Safety in Karst Area, Guilin University of Technology, Guilin 541004, China*
[d]*Faculty of Hydrology and Water Resources Engineering, Institute of Technology of Cambodia, Phnom Penh 120000, Cambodia*

Received 14 July 2018; Accepted 27 December 2018

ABSTRACT

A commercial bentonite was modified by Al/Mg-polymeric hydroxy, and its potential application of removing Cu^{2+}, Cd^{2+}, and Pb^{2+} from aqueous solution was also discussed. The modification did not change the bentonite microstructure, while the surface morphology becomes rough and the methyl and methylene groups appeared on the surface of modified bentonite (B-Al/Mg). Under acidic condition, the removal of Cu^{2+}, Cd^{2+}, and Pb^{2+} raised with the increase of initial pH of solutions, media dosage, and reaction temperature, and the efficacious contact times for Cu^{2+}, Cd^{2+}, and Pb^{2+} removal were 6 (Cu^{2+}) and 8 h (Cd^{2+} and Pb^{2+}). The Cu^{2+}, Cd^{2+}, and Pb^{2+} adsorption processes could be better described by Freundlich isotherm model and pseudo-second-order model. The intraparticle diffusion might be the rate-controlling step of Cu^{2+} and Pb^{2+} adsorption. The Cu^{2+}, Cd^{2+}, and Pb^{2+} adsorptions were heterogeneous, spontaneous, endothermic, and irreversible processes. The adsorptions of Cu^{2+} and Cd^{2+} were dominated by physisorption, while the chemisorption was dominant in Pb^{2+} adsorption. The results of column experiments suggested that B-Al/Mg had the potential application in purification of drinking water in practice because its removal of Cu^{2+}, Cd^{2+}, and Pb^{2+} was greater than activated carbons selected in this study, and the breakthrough times were up to 20–30 d. Simultaneously, the heavy metal concentrations of outlet were all less than the World Health Organization standard in breakthrough time. The dynamic adsorption of $Cu2^{+}$, Cd^{2+}, and Pb^{2+} was well described by bed-depth service time model. B-Al/Mg had the potential for commercial applications. For single heavy metal removal, the advised adsorption columns were column 4 (Cu^{2+} and Pb^{2+}) and column 1 (Cd^{2+}), and the column 5 was suggested for Cu^{2+}, Cd^{2+}, and Pb^{2+} competitive adsorption.

Keywords: Bentonite modification; Al/Mg-hydroxyl polymerization; Heavy metal removal; Adsorption

1. Introduction

Due to the rapid industrialization, large amounts of heavy metals are discharged into the surface water and groundwater sources [1], causing serious health risks to humans [2]. The heavy metals in water are mainly Cu^{2+}, Cd^{2+}, Ni^{2+}, Mn^{2+}, Pb^{2+}, Hg^{2+}, and so on [3–6]. Among them, the Cd^{2+} and Pb^{2+} are more toxic to humans and could result in abnormalities of muscle and nerve and organ failure [7]. Therefore, US Environmental Protection Agency and World

* Corresponding authors.

Health Organization (WHO) strictly limit the concentrations of Cd^{2+} and Pb^{2+} in drinking water [8]. In addition, trace amounts of Cu^{2+} in the water also cause serious damage to the brain of humans or animals [9]. Hence, it is very necessary to remove Cd^{2+}, Pb^{2+}, and Cu^{2+} from the water for the safety of drinking water.

In the past decades, various technologies, such as biosorption [4], adsorption [10], ion exchange of membrane and resin [11], coagulation, and sedimentation [2], have been developed for heavy metal removal. Due to its simplicity and efficiency, adsorption is often the preferred solution. Among the adsorbents commonly used in adsorption, modified bentonites have been proven to have better removal of heavy metals in solutions [12–14]. At present, the agents used for the modification of bentonite mainly include inorganic and organic acids, organic compounds, metals, and salts [12,15–19]. However, there are almost no reports on the modification of bentonite by Al/Mg-polymeric hydroxy.

In this study, a commercial bentonite was modified by Al-Mg-hydroxyl polymerization, and then the potential of modified bentonite for Cd^{2+}, Pb^{2+}, and Cu^{2+} removal from aqueous solutions was also evaluated by static experiments and dynamic column experiments.

2. Materials and methods

2.1. Materials

The bentonite used in experiments is from Zhengzhou, China, and its basic properties are as follows: Expansion capacity 7.5 mL/g, Glue medium 10.4 mL/g, Methylene blue adsorption 0.601 mmol/g, and Cation-exchange capacity 9.69 cmol/kg. The chemical reagents $(NaPO_3)_6$, Na_2CO_3, $AlCl_3$, NaOH, $MgCl_2$, $CuSO_4$, $Cd(NO_3)_2$, and $Pb(NO_3)_2$ are all AR.

2.2. Preparation of modified bentonite

2.2.1. Purification of bentonite

First, the pH value of 0.04 mol/L $(NaPO_3)_6$ solution was adjusted to 7 with 4% Na_2CO_3 solution. Second, 200 g of bentonite was added to 200 mL of the above solution and stirred for 0.5 h at 60°C. After standing for 1.5 h, the upper suspension was dried at 105°C and pulverized through a 200 mesh sieve.

2.2.2. Preparation of Al/Mg-polymerized hydroxyl

First, 0.1 mol/L NaOH solution and 0.1 mol/L $AlCl_3$ solution were mixed at 80°C and continuously stirred for 3 h. And then, the mixture was aged for 24 h at 80°C. Afterward, 0.1 mol/L $MgCl_2$ solution was added into the aged mixture with the Mg^{2+} and Al^{3+} molar ratio of 0.1. Similarly, the new mixture was also stirred and aged under the above conditions.

2.2.3. Modification of bentonite

The purified bentonite was prepared as a suspension of 3 g/L and stirred for 3 h at 50°C. Then the Al/Mg-polymerized hydroxyl was continuously dripped into the suspension at 90°C, until the ratio of the molar amount of Mg^{2+}/Al^{3+} to the mass of bentonite was 1 mmol/g. After these, the mixture was aged for 36 h at the same temperature. Then, the aged mixture was centrifugally cleaned several times to obtain modified bentonite. Finally, the modified bentonite was activated for 2 h at 105°C and also pulverized through a 200 mesh sieve. And the modified bentonite was named as B-Al/Mg.

2.3. Characterization of modified bentonite

The surface topography and crystal structure of raw and modified bentonites were detected using scanning electron microscope (SEM) (JEOL, JSM-6380LV) and X-ray diffraction (XRD) (PANalytical, Xpert Pro), respectively. Fourier transform infrared spectroscopy (FTIR, Thermo Nicolet 470FT-IR) was also used to identify the surface functional groups of the two samples.

2.4. Adsorption experiments

2.4.1. Static adsorption experiments

In this section, the effects of adsorbent dosages, adsorption temperature, contact time, and initial pH on Cd^{2+}, Pb^{2+}, and Cu^{2+} removal were investigated. Modified bentonite with different qualities was added into 100-mL centrifuge tubes filled with 30 mL heavy metal solutions of concentration of 50 mg/L. The centrifuge tubes were vibrated at 240 rpm. After centrifugation, the heavy metal concentrations in supernatant were measured by an inductively coupled plasma atomic emission spectrometer (Optima 7000DV). The removal efficiency ϕ (%) of heavy metals was calculated by the following equation:

$$\phi = \frac{(C_0 - C)}{C_0} \times 100\% \quad (1)$$

where C_0 and C (mg/g) are the concentrations of initial and adsorption ends, respectively.

2.4.2. Dynamic adsorption experiments

In order to evaluate the potential of modified bentonite for Cd^{2+}, Pb^{2+}, and Cu^{2+} removal from aqueous solutions, seven column experiments were run in parallel in the laboratory scale. The process of the column experiments is shown in Fig. 1. The details of these columns were as follows: 30% quartz sand + 70% B-Al/Mg for column 1; 30% quartz sand + 50% B-Al/Mg + 20% commercial activated carbon for column 2; 30% quartz sand + 30% B-Al/Mg + 40% commercial activated carbon for column 3; 30% quartz sand + 10% B-Al/Mg + 60% commercial activated carbon for column 4; 30% quartz sand + 30% B-Al/Mg + 30% commercial activated carbon + 10% iron powder for column 5; 30% quartz sand + 70% commercial activated carbon for column 6; and 100% quartz sand for column 7. The percentages are mass percents. The analog drinking water containing heavy metal of 40 mg/L in storage tank was pumped into column by metering pump with the flow rate

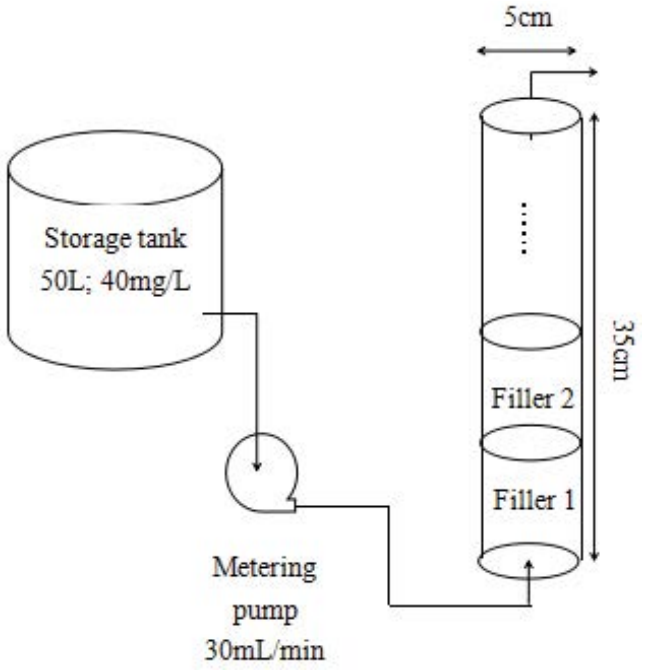

Fig. 1. The process of column experiment.

of 30 mL/min. The heavy metal concentrations and removal rate of the outlet were also determined by the methods in the section "Static adsorption experiments."

3. Results and discussion

3.1. Characterization of B-Al/Mg

Figs. 2, 3, and 4 show the characterization results of raw bentonite and B-Al/Mg by XRD, FTIR, and SEM, respectively. From Fig. 2, it can be seen that the two patterns are quite similar, suggesting that the material structure has not been destroyed by modification. And the significant peaks of B-Al/Mg are relatively small, which indicates that the B-Al/Mg has less impurities. Based on XRD data, the main components of B-Al/Mg and raw bentonite are montmorillonite and quartz, while dolomite and kaolinite are also present in small amounts [14,16,20].

As Fig. 3 shows, the difference between raw bentonite and B-Al/Mg is mainly concentrated in two wave ranges of 2,900–3,000 and 1,200–1,800 cm^{-1}, respectively. The unique feature bands of B-Al/Mg around 3,000, 2,900, and 1,800 cm^{-1} are assigned to –CH asymmetric stretching vibration, bending vibration of $–CH_2$, and C=O stretches, respectively [21–23]. The consistent bands of the two bentonites around 3,650, 3,450, 1,650, 1,050, and 500 cm^{-1} are attributed to Al(Mg)–OH stretching, υ–H–OH of adsorbed water, stretching vibration of –FeOO–, stretching vibration of Si–O–Si, and stretching vibration of Al–Mg–OH, respectively [22].

The surface of raw bentonite is obviously lamellar and relatively smooth, while there are obvious signs of erosion and attached small particles on the surface of B-Al/Mg (Fig. 4). These indicate that Al/Mg-hydroxyl polymerization has a strong etch effect [20].

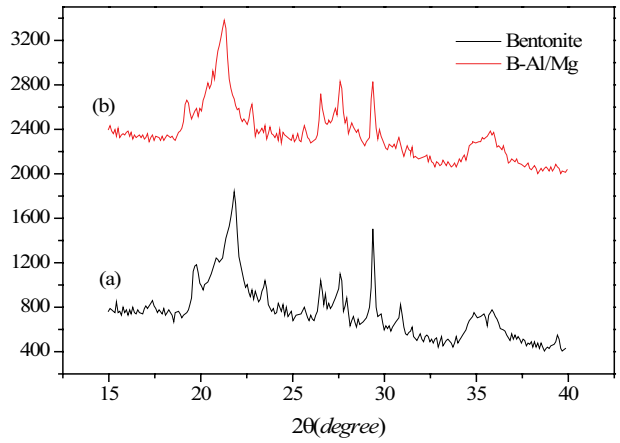

Fig. 2. The XRD patterns of raw bentonite (a) and B-Al/Mg (b).

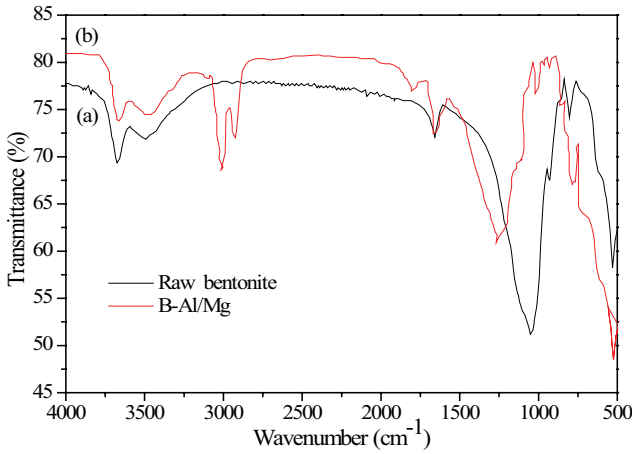

Fig. 3. FTIR spectra of raw bentonite (a) and B-Al/Mg (b).

3.2. Effect of operational parameters on Cu^{2+}, Cd^{2+}, and Pb^{2+} removal

3.2.1. Effect of initial pH

Because of the strong effect on the media surface [24], the initial pH of the solution is generally the primary control parameter. The effect of solution pH values on Cd^{2+}, Pb^{2+}, and Cu^{2+} removal is shown in Fig. 5(a). In the pH range of 1–5, the removal of Cd^{2+}, Pb^{2+}, and Cu^{2+} has risen with the increase of pH, which are consistent with the study of Ahmad and Hasan [12]. This may be due to the increase in the number of negative charges on the surface of B-Al/Mg [25]. And the pH_{PZC} of B-Al/Mg measured by weight method [24] is about 6.2 (Fig. 5(b)), which also indicates that higher pH value of solution favors the adsorptions of Cd^{2+}, Pb^{2+}, and Cu^{2+} on B-Al/Mg.

3.2.2. Effect of adsorbent dosage

Due to increase in adsorption or ion-exchange sites, more adsorbent could improve the removal of heavy metals [14]. As Fig. 6 shows, the variation tendencies of Cd^{2+}, Pb^{2+}, and Cu^{2+} removal are all ascendant with the raising adsorbent dosages. Comparing Cu^{2+} and Cd^{2+}, the lower adsorbent

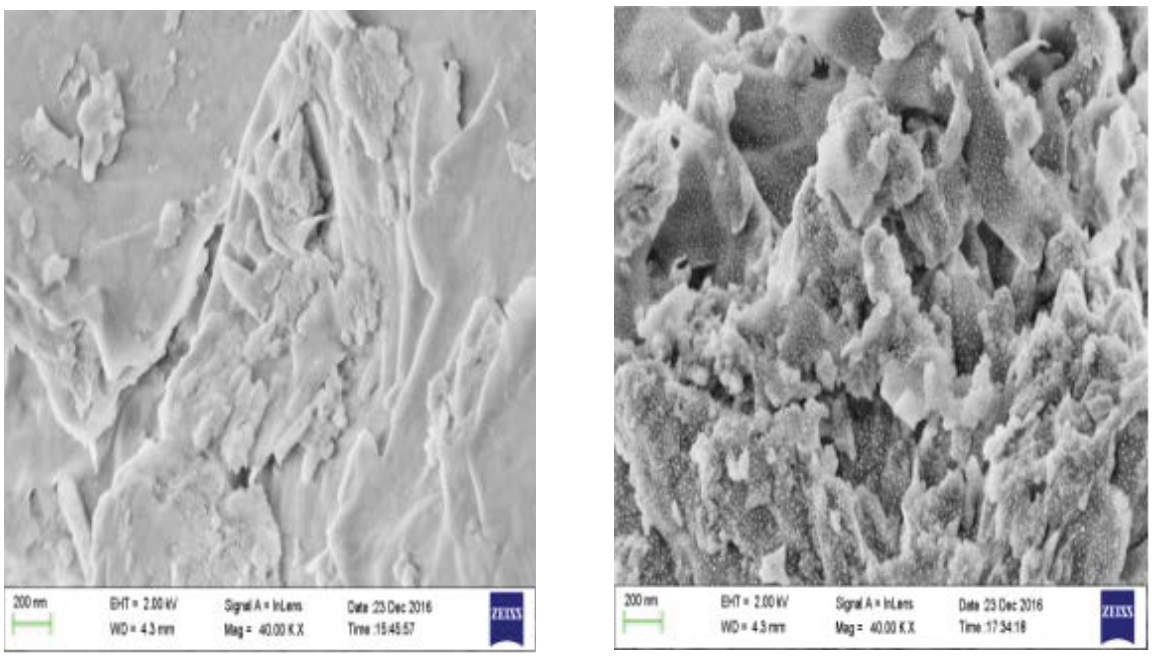

Fig. 4. The SEM images of raw bentonite (left) and B-Al/Mg (right).

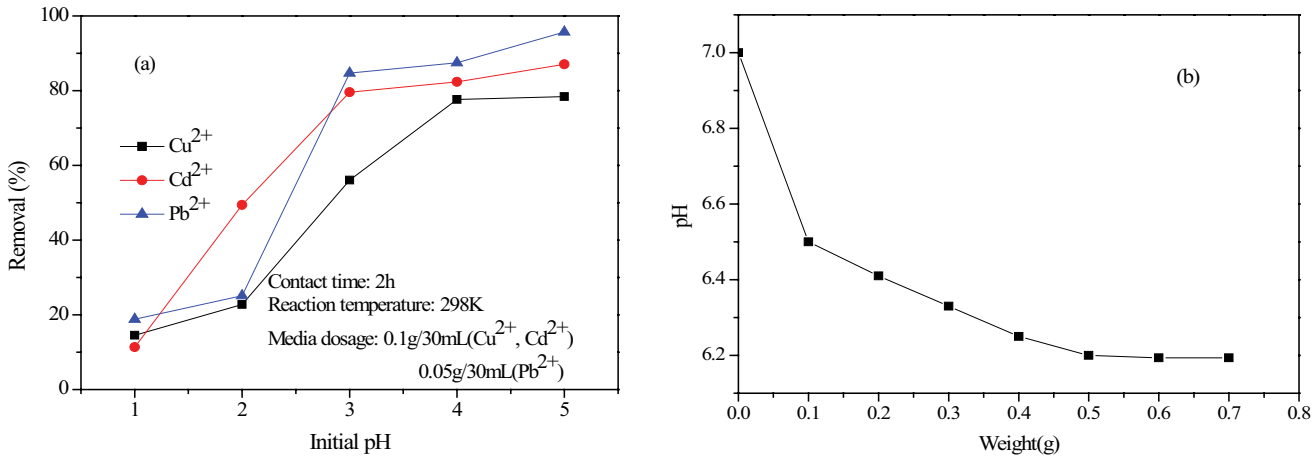

Fig. 5. The effect of initial pH on Cd^{2+}, Pb^{2+}, and Cu^{2+} removal (a) and the point of zero charge for B-Al/Mg (b).

dosages will allow the removal rate of Pb^{2+} to reach a higher level, indirectly indicating that B-Al/Mg may be more beneficial for adsorption of Pb^{2+}.

3.2.3. Effect of contact time

Generally, the removal of heavy metals is quickly increased in the initial short time, and then this tendency becomes very slow [26]. This is due to the change of adsorption sites on the adsorbent surface [27]. From Fig. 7, it can be seen that when the contact times are less than 6 and 8 h, respectively, the removal of Cd^{2+}, Pb^{2+}, and Cu^{2+} follows the above regular pattern. However, with the further extension of contact time, there are different degrees of reductions of removal. This suggests that the favorable contact times are 6 (Cd^{2+}) and 8 h (Cu^{2+} and Pb^{2+}).

3.2.4. Effect of adsorption temperature

The effects of reaction temperature on heavy metal removal are shown in Fig. 8. An obvious increase of removal can be noticed in the range of 283–313 K. This indicates that the removal of Cd^{2+}, Pb^{2+}, and Cu^{2+} is an endothermic process [28]. At high temperature, the heavy metal ion movement becomes intense, resulting in the improvement of collision and reaction between adsorbates and adsorbents.

3.3. Isotherms, kinetics, and thermodynamics of Cu^{2+}, Cd^{2+}, and Pb^{2+} adsorption

3.3.1. Adsorption isotherms

In order to discuss the isothermal adsorption of Cu^{2+}, Cd^{2+}, and Pb^{2+} on B-Al/Mg, experiments on the effects of

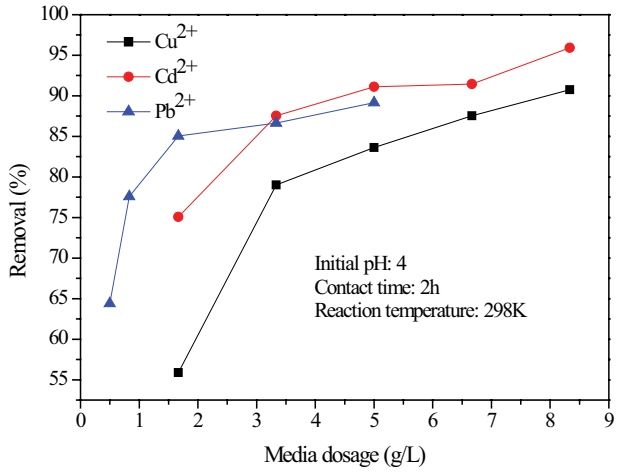

Fig. 6. The effect of adsorbent dosages on Cd^{2+}, Pb^{2+}, and Cu^{2+} removal.

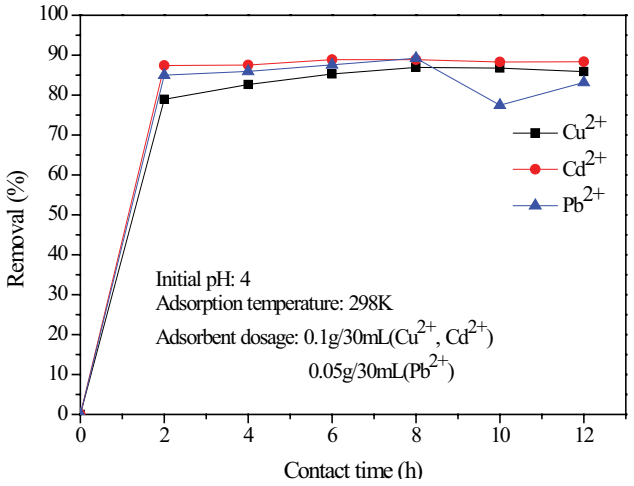

Fig. 7. The effect of contact time on Cd^{2+}, Pb^{2+}, and Cu^{2+} removal.

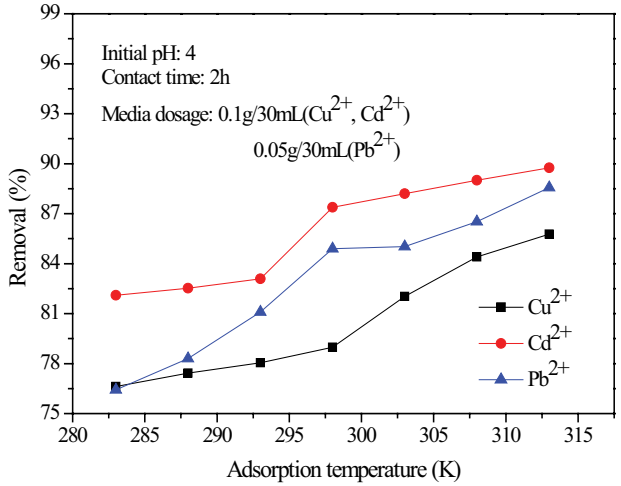

Fig. 8. The effect of adsorption temperature on Cd^{2+}, Pb^{2+}, and Cu^{2+} removal.

initial concentrations of Cu^{2+}, Cd^{2+}, and Pb^{2+} on removal rates were performed. The results are shown in Fig. 9(a). It can be seen that with the increase of initial concentration, the removal rates of Cu^{2+}, Cd^{2+}, and Pb^{2+} are decreased. And then the Langmuir, Freundlich, and Temkin isotherm models were used to analyze the adsorption data. The linear expressions of the three isotherms are as follows [20,24]:

Langmuir isotherm

$$\frac{C_e}{q_e} = \frac{1}{q_{\max} K_L} + \frac{C_e}{q_{\max}} \tag{2}$$

Freundlich isotherm

$$\log q_e = \log K_F + \frac{1}{n} \log C_e \tag{3}$$

Temkin isotherm

$$q_e = \frac{RT}{b_T} \ln K_T + \frac{RT}{b_T} \ln C_e \tag{4}$$

where q_e (mg/g) is the adsorption amount at equilibrium, which is calculated by the following equation: $q_e = (C_0 - C_e)\, V/W$, where C_e (mg/L) is ion concentration at equilibrium, V(L) and W(g) are solution volume and adsorbent dosage, respectively, $q_{\max}$ (mg/g) is the maximum adsorption capacity of the adsorbent, K_L (L/mg) is the Langmuir constant related to the adsorption capacity and adsorption rate; K_F ((mg/g)(mg/L)$^{1/n}$) and n are the Freundlich constants related to adsorption capacity and intensity, respectively, b_T (J/mol) is the Temkin constant related to the heat of adsorption, K_T (L/mg) is the Temkin isotherm constant, T (K) is the absolute temperature, and R is the universal gas constant.

The linear fitting results are presented in Figs. 9(b)–(d). And the constants of the three isotherm equations are listed in Table 1. It is clear that the R^2 values of Freundlich isotherm are greater than 0.99, suggesting that Cu^{2+}, Cd^{2+}, and Pb^{2+} adsorption on to B-Al/Mg is a heterogeneous adsorption process. And the n values of Freundlich isotherm are all in the range of 1–10 indicating that the Cu^{2+}, Cd^{2+}, and Pb^{2+} adsorption is preferential. Furthermore, the R^2 values of Temkin isotherm are around 0.90, which means the adsorption of Cu^{2+}, Cd^{2+}, and Pb^{2+} may be a chemical adsorption-based process.

3.3.2. Adsorption kinetics

To clarify the rate-limiting mass transfer mechanisms and to evaluate the characteristic mass transfer parameters, the pseudo-first-order, pseudo-second-order, and intraparticle diffusion models [29] were used to fit the data shown in Fig. 7. The mathematical expressions of the four models are presented as

pseudo-first-order model

$$\log\left(q_e - q_t\right) = \log q_e - k_1 t \tag{5}$$

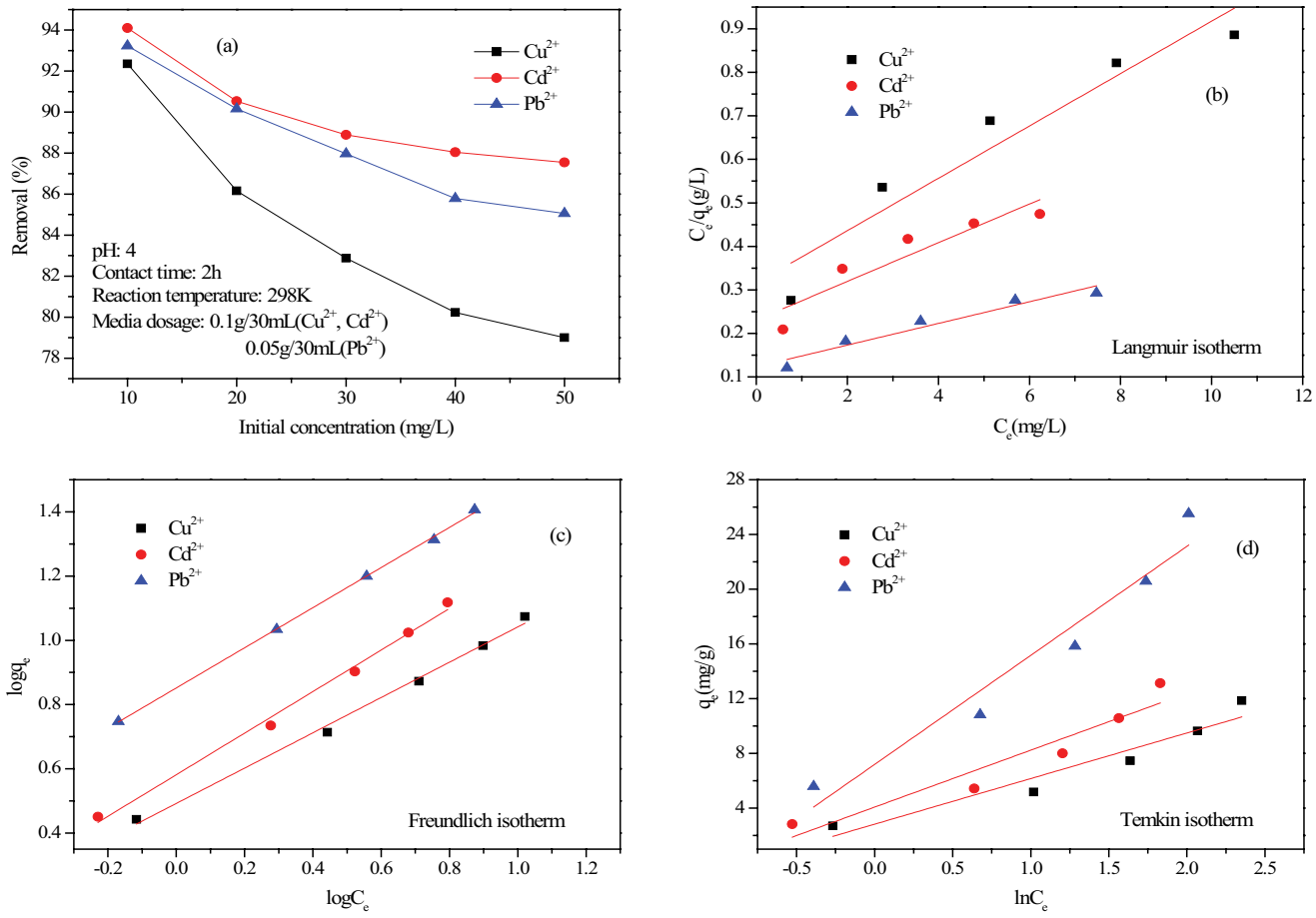

Fig. 9. The effect of initial concentration on Cd^{2+}, Pb^{2+}, and Cu^{2+} removal (a) and adsorption isotherms for Cu^{2+}, Cd^{2+}, and Pb^{2+} (b, c, d).

pseudo-second-order model

$$\frac{t}{q_t} = \frac{1}{k_2 q_e^2} + \frac{t}{q_e} \tag{6}$$

intraparticle diffusion model

$$q_t = k_i t^{0.5} + C \tag{7}$$

where q_t (mg/g) is the adsorption amount at time t, which is calculated by the following equation: $q_t = (C_0 - C_t)\ V/W$, where C_t (mg/L) is ion concentration at time t, k_1 (1/h) is the pseudo-first-order rate constant, k_2 (g/(mg h)) is the relevant adsorption rate constant of pseudo-second order, k_i (mg/(g $h^{0.5}$)) is the constant of intraparticle diffusion rate, and C is the intercept, representing the thickness effects of the boundary layer.

The fitting results and kinetic parameters are shown in Fig. 10 and Table 2, respectively. It is obvious that the adsorption processes of Cu^{2+}, Cd^{2+}, and Pb^{2+} are more consistent with the pseudo-second-order model because the R^2 values of the pseudo-second-order kinetic model are higher than the other two models and are greater than 0.98. And the equilibrium adsorption amounts of Cu^{2+}, Cd^{2+}, and Pb^{2+} calculated by the quasi-second-order kinetic model ($q_{e2,cal}$) are very close to the experimental values ($q_{e,exp}$). For Cu^{2+} and Pb^{2+}, intraparticle diffusion may be the potential rate-controlling step, since their R^2 values of the intraparticle diffusion model are both greater than 0.90. However, because the C values are greater than zero, there may be thickness effect in the boundary layer in Cu^{2+} and Pb^{2+} adsorption processes.

3.3.3. Adsorption thermodynamics

According to the data in Fig. 8, the changes of Gibbs free energy (ΔG), enthalpy (ΔH), and entropy (ΔS) were calculated by Eqs. (8)–(10) [24], in order to assess the adsorption heat of Cu^{2+}, Cd^{2+}, and Pb^{2+} adsorption.

$$\Delta G = \Delta H - T\Delta S \tag{8}$$

$$\Delta G = -RT \ln K_d \tag{9}$$

$$K_d = q_e \frac{\left(\frac{W}{V}\right)}{C_e} \tag{10}$$

Table 1
Isotherm parameters of Cu^{2+}, Cd^{2+}, and Pb^{2+} adsorption on B-Al/Mg

Ions	$q_{max,exp}$	Langmuir isotherm			Freundlich isotherm			Temkin isotherm		
		q_{max}	K_L	R^2	K_F	n	R^2	b_T	K_T	R^2
Cu^{2+}	11.85	16.61	0.1907	0.8944	3.107	1.820	0.9936	743.6	2.335	0.9025
Cd^{2+}	13.13	22.47	0.1930	0.8236	3.817	1.546	0.9914	595.7	2.663	0.8825
Pb^{2+}	25.52	40.16	0.2019	0.9275	7.109	1.601	0.9991	310.9	2.465	0.9275

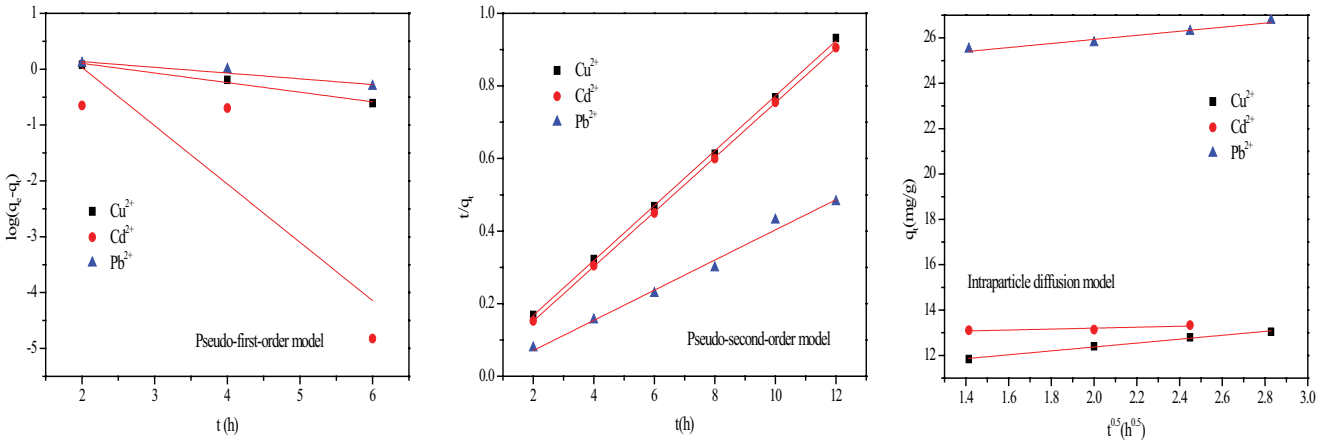

Fig. 10. Kinetic plots of Cu^{2+}, Cd^{2+}, and Pb^{2+} adsorption on B-Al/Mg.

Table 2
Kinetic parameters of Cu^{2+}, Cd^{2+}, and Pb^{2+} adsorption on B-Al/Mg

Ions	$q_{e,exp}$ (mg/g)	Pseudo-first-order model			Pseudo-second-order model			Intraparticle diffusion model		
		$q_{e1,cal}$ (mg/g)	k_1 (1/h)	R^2	$q_{e2,cal}$ (mg/g)	k_2 (g/(mg h))	R^2	k_i (mg/(g $h^{0.5}$))	C	R^2
Cu^{2+}	13.04	2.808	0.1721	0.9714	13.21	0.3582	0.9995	0.8600	10.65	0.9914
Cd^{2+}	13.34	131.2	1.044	0.5164	13.30	4.284	0.9999	0.2078	12.79	0.5258
Pb^{2+}	26.78	2.194	0.1027	0.8654	24.27	0.1319	0.9861	0.8981	24.14	0.9313

where ΔG (kJ/mol) is the Gibbs free energy change, ΔH (kJ/mol) is the change in enthalpy, ΔS (J/(mol.K)) is the change in entropy, K_d is the distribution coefficient of adsorption, R (8.314 J/(mol K)) is the universal gas constant, and T (K) is Kelvin temperature.

The results are shown in Table 3. The negative ΔG values suggest that the Cu^{2+}, Cd^{2+}, and Pb^{2+} adsorptions onto B-Al/Mg are spontaneous [14]. As the temperature increases, a decrease in ΔG values indicates that high temperature is more favorable for Cu^{2+}, Cd^{2+}, and Pb^{2+} adsorptions [2]. The positive values of ΔS reveal disorderliness at the solid/solution interface during the adsorption processes of Cu^{2+}, Cd^{2+}, and Pb^{2+} onto B-Al/Mg, while the positive values of ΔH indicate that the processes of Cu^{2+}, Cd^{2+}, and Pb^{2+} adsorptions are endothermic and irreversible [28]. In addition, the ΔH values of Cu^{2+}, Cd^{2+}, and Pb^{2+} adsorption processes also indicate that the adsorptions of Cu^{2+} and Cd^{2+} are dominated by physisorption, while the chemisorption is dominant in Pb^{2+} adsorption [24].

3.4. The potential application of B-Al/Mg in practice

3.4.1. Removal of single heavy metal

Fig. 11 shows the running results of column experiments in 60 d for Cd^{2+}, Pb^{2+}, and Cu^{2+}. Some preliminary conclusions can be obtained and are shown as below: (1) there was almost no effect on the removal of Cd^{2+}, Pb^{2+}, and Cu^{2+} for quartz sands; (2) the removal of B-Al/Mg for Cd^{2+}, Pb^{2+}, and Cu^{2+} are greater than activated carbons, and the mixing medium is better for heavy metal removal; (3) the addition of iron powder is beneficial for Cd^{2+}, Pb^{2+}, and Cu^{2+} removal due to the chemical reactions between Fe and heavy metal ions; (4) the breakthrough times of B-Al/Mg which is defined as the time when the heavy metal concentrations are beyond the WHO standard; in this study for Cu^{2+}, Cd^{2+}, and Pb^{2+}, the breakthrough times are 23, 25, and 31 d, respectively, that are much higher than the previous reports [4,7]. These evidences suggest that B-Al/Mg has the potential to treat drinking water contaminated by Cu^{2+}, Cd^{2+}, or Pb^{2+} in practice.

Table 3
Thermodynamic parameters of Cu^{2+}, Cd^{2+}, and Pb^{2+} adsorption on B-Al/Mg

Ions	ΔH (kJ/mol)	ΔS (J/mol)	ΔG (kJ/mol)							R^2
			283 K	288 K	293 K	298 K	303 K	308 K	313 K	
Cu^{2+}	15.86	65.16	–2.793	–2.951	–3.090	–3.280	–3.826	–4.323	–4.674	0.9316
Cd^{2+}	18.10	76.09	–3.583	–3.718	–3.878	–4.795	–5.066	–5.355	–5.647	0.9442
Pb^{2+}	21.27	84.85	–2.768	–3.072	–3.548	–4.278	–4.374	–4.760	–5.328	0.9774

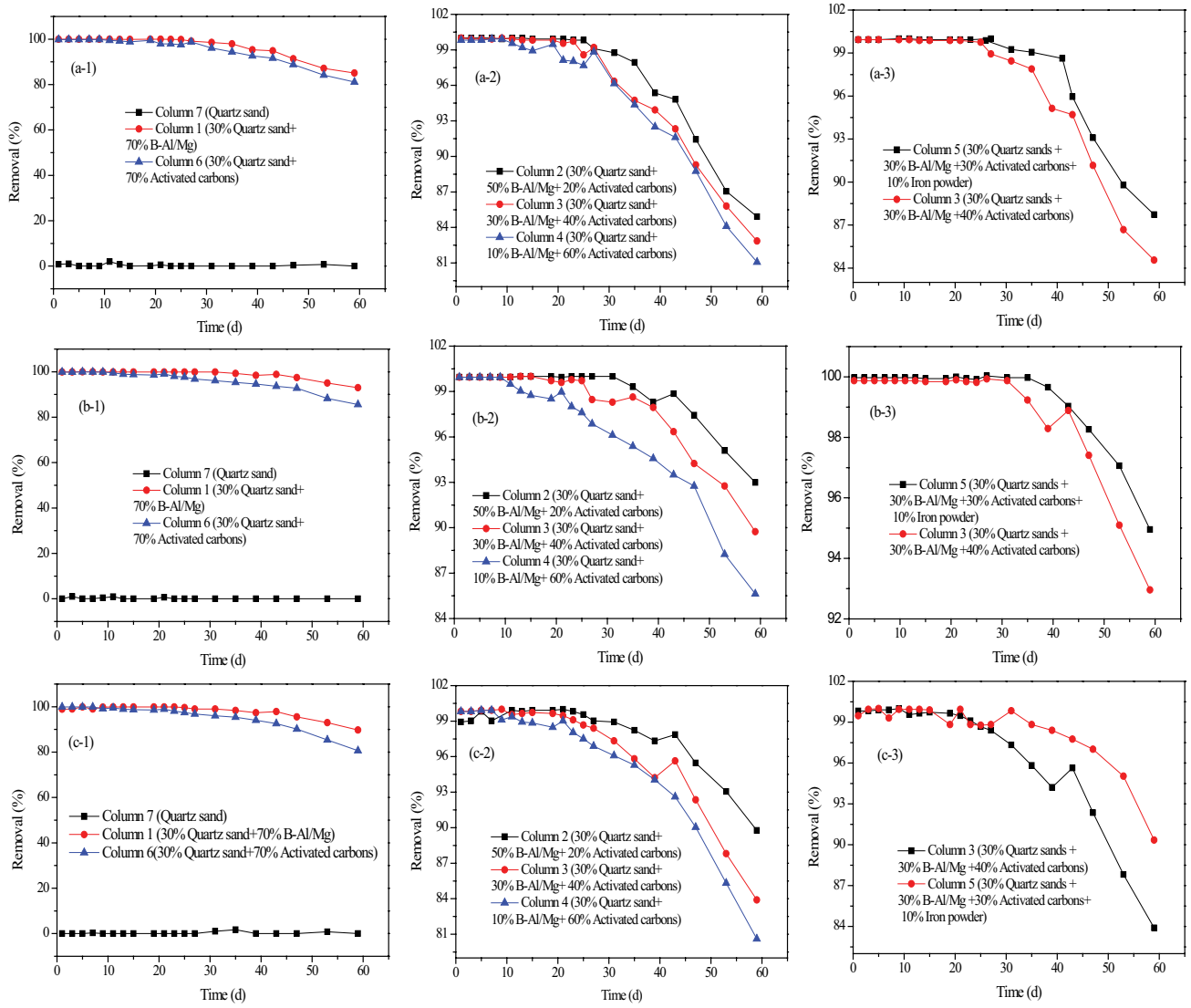

Fig. 11. The column experimental results of Cu^{2+}, Cd^{2+}, and Pb^{2+} removal: (a) Cu^{2+} removal, (b) Cd^{2+} removal, and (c) Pb^{2+} removal.

3.4.2. Removal of multiple heavy metals

Since quartz sand plays useless role in the removal of heavy metals, it is not discussed in this section. Fig. 12 shows the removal of Cu^{2+}, Cd^{2+}, and Pb^{2+} from their mixtures by the other six columns. It is clear that they all have rather good effect to simultaneously remove Cu^{2+}, Cd^{2+}, and Pb^{2+}. In the early stage, the removal of heavy metals is very close to 100% and then gradually decreases with the increase of running time. Since the adsorption or ion-exchange sites are rapidly occupied, the breakthrough times have reduced. Similarly, the addition of iron powder could effectively improve removal efficiency of heavy metals and delay breakthrough times. Meanwhile, the order of the three heavy metal removal rates is $Pb^{2+} > Cu^{2+} > Cd^{2+}$, suggesting that the Pb^{2+} is preferentially removed. Therefore, the

B-Al/Mg also has the potential application in purification of multiple heavy metal-contaminated drinking water, and the process of column 5 experiment is advised. However, there is a very important explanation. In all column experiments, when the running time is more than about 15 d, there will be a significant reduction in the permeability of the cylinder due to the expansion of B-Al/Mg. This will limit the application of B-Al/Mg in the treatment of drinking water heavily polluted with Cu^{2+}, Cd^{2+}, and Pb^{2+} in practice.

3.4.3. Adsorption dynamics in fixed-bed columns

Adsorption models of fixed-bed columns mainly include Thomas model, Adams-Bohart model, Yoon-Nelson model, and bed-depth service time (BDST) model [30]. In this study, BDST model was selected to discuss the data of Cu^{2+}, Cd^{2+}, and Pb^{2+} removal in six fixed-bed columns. The linear mathematical expression of BDST model is as follows [31]:

$$t = \frac{N_0}{C_0 F} Z - \frac{1}{k_a C_0} \ln\left(\frac{C_0}{C_t} - 1\right) \tag{11}$$

where F (m/d) is the influent linear velocity and could be calculated from the flow rate and the cross-sectional area of the column, N_0 (g/L) is the adsorption capacity, Z (m) is the effective height of the adsorption column, k_a (L/g d) is the rate constant in the BDST model.

According to the data shown in Fig. 11, the fitting results and parameters of BDST model for Cu^{2+}, Cd^{2+}, and Pb^{2+} removal in different columns are presented in Fig. 13 and Table 4, respectively. It can be seen that the dynamic

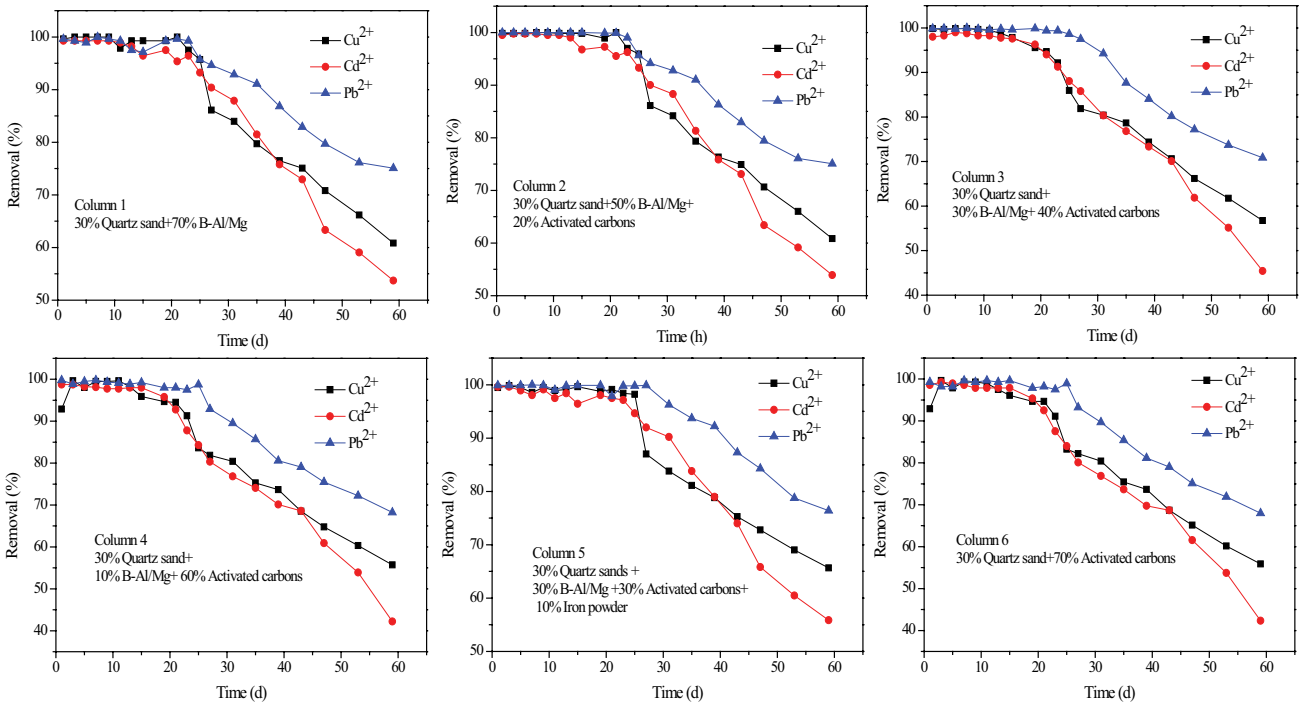

Fig. 12. The removal of Cu^{2+}, Cd^{2+}, and Pb^{2+} from their mixture in different column experiments.

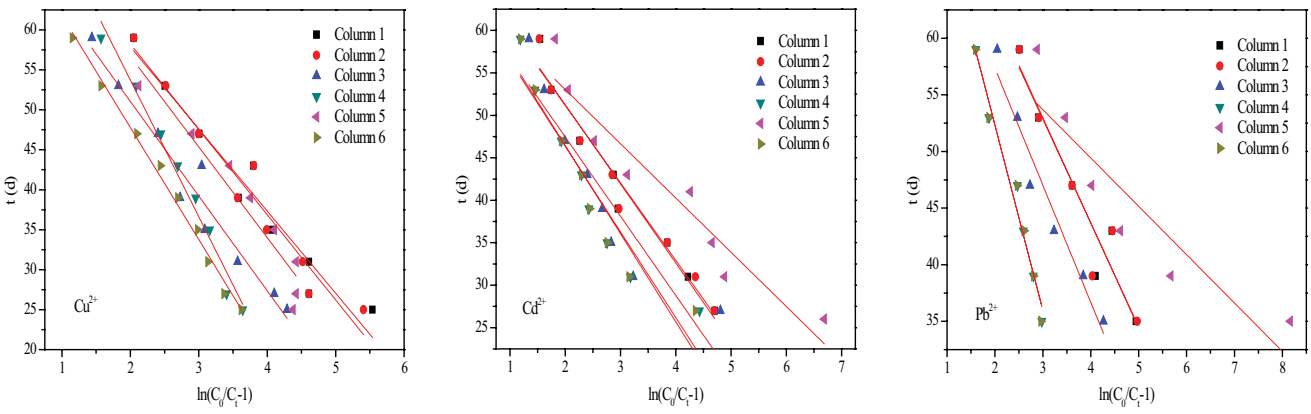

Fig. 13. The linear fitting of BDST model for Cu^{2+}, Cd^{2+}, and Pb^{2+} breakthrough curves.

Table 4
The parameters of BDST model for Cu^{2+}, Cd^{2+}, and Pb^{2+} removal in different columns

Column number	Cu^{2+}			Cd^{2+}			Pb^{2+}		
	K_a (L/(g d))	N_0 (g/L)	R^2	K_a (L/(g d))	N_0 (g/L)	R^2	K_a (L/(g d))	N_0 (g/L)	R^2
1	2.433	197.2	0.9433	2.687	175.6	0.9593	2.692	203.2	0.9103
2	2.343	200.1	0.9477	2.739	174.6	0.9592	2.728	202.0	0.8925
3	2.111	187.9	0.9512	2.679	166.2	0.8353	2.411	196.2	0.9477
4	1.463	221.0	0.9786	2.478	167.3	0.8844	1.528	213.8	0.9705
5	2.203	199.6	0.9086	3.913	165.5	0.9093	5.855	167.2	0.7907
6	1.781	190.7	0.9911	2.411	168.9	0.8940	1.530	213.7	0.9680

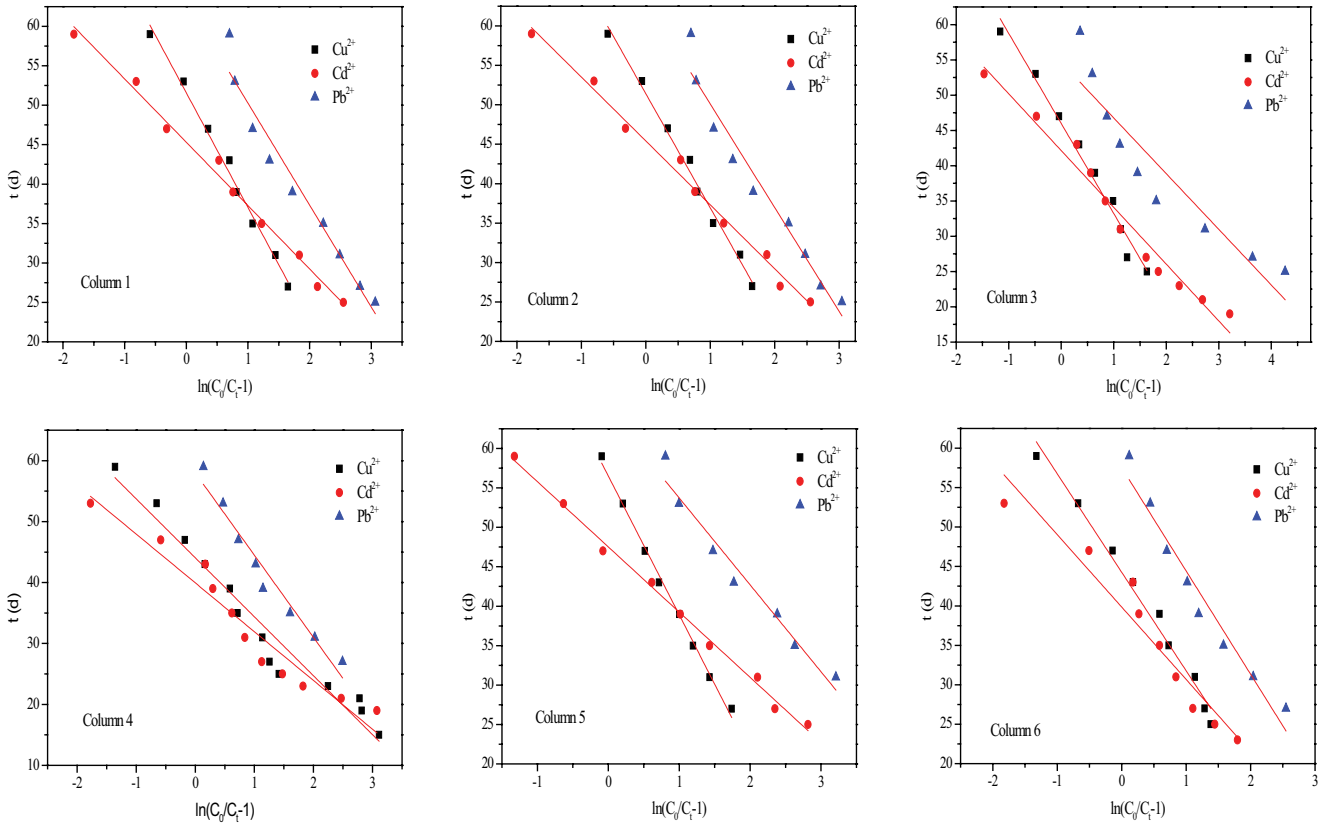

Fig. 14. The linear fitting of BDST model for Cu^{2+}, Cd^{2+}, and Pb^{2+} competitive adsorption process.

Table 5
The parameters of BDST model for Cu^{2+}, Cd^{2+}, and Pb^{2+} competitive adsorption

Column number	K_a (L/(g d))			N_0 (g/L)				R^2		
	Cu^{2+}	Cd^{2+}	Pb^{2+}	Cu^{2+}	Cd^{2+}	Pb^{2+}	Total	Cu^{2+}	Cd^{2+}	Pb^{2+}
1	5.158	9.336	5.800	43.23	37.97	52.97	134.2	0.9905	0.9909	0.9553
2	5.181	9.256	5.699	43.08	38.06	53.03	134.2	0.9900	0.9895	0.9516
3	5.876	9.318	9.503	38.54	35.32	45.80	119.7	0.9800	0.9678	0.8563
4	7.754	9.367	5.559	36.93	33.48	48.60	119.0	0.9542	0.9320	0.9527
5	4.263	9.070	6.806	47.36	39.82	54.26	141.4	0.9952	0.9947	0.9571
6	6.005	8.168	5.729	37.10	33.40	48.21	118.7	0.9835	0.9262	0.9532

adsorption process of Cu^{2+}, Cd^{2+}, and Pb^{2+} on different adsorption columns can be well described by BDST model. Comparing column 1 and column 6, the adsorption capacities of Cu^{2+} and Cd^{2+} on B-Al/Mg adsorption column are higher than that of commercial activated carbon and the adsorption capacity of Pb^{2+} is very close to commercial activated carbon. This indicates that B-Al/Mg has the potential for commercial applications. For Cu^{2+} and Pb^{2+} removal, the column 4 is advised, while the column 1 is more advantageous for Cd^{2+} removal.

Fig. 14 and Table 5 show the fitting results and parameters of BSDT model for the dynamic competitive adsorption process of Cu^{2+}, Cd^{2+}, and Pb^{2+} on different adsorption columns (Fig. 12), respectively. It is obvious that the competitive adsorption processes can also be well described by the BDST model. Due to competition for the adsorbed active sites, the total adsorption capacities of the three ions on different columns are lower than that of the single ion. In contrast, Cd^{2+} is more easily adsorbed and removed. Moreover, column 5 has a better removal on the three ions.

4. Conclusions

A commercial bentonite was modified by Al/Mg-polymeric hydroxy, and then it was used for the removal of Cu^{2+}, Cd^{2+}, and Pb^{2+}. The characterization of raw and modified bentonites showed that the modification did not change the bentonite microstructure, while the surface morphology becomes rough and the methyl and methylene groups appeared on the surface of modified bentonite. Under acidic condition, the removal of Cu^{2+}, Cd^{2+}, and Pb^{2+} raised with the increase of initial pH of solution, adsorbent dosage, and adsorption temperature, and the efficacious contact times for Cu^{2+}, Cd^{2+}, and Pb^{2+} removal were 6 (Cu^{2+}) and 8 h (Cd^{2+} and Pb^{2+}). The removal of Cu^{2+}, Cd^{2+}, and Pb^{2+} under the relative optimization conditions was close or beyond 90%. The isotherms, kinetics, and thermodynamics of Cu^{2+}, Cd^{2+}, and Pb^{2+} adsorption showed that the Cu^{2+}, Cd^{2+}, and Pb^{2+} adsorption processes could be better described by Freundlich isotherm model and pseudo-second-order model. The intraparticle diffusion might be the rate-controlling step of Cu^{2+} and Pb^{2+} adsorption. Cu^{2+}, Cd^{2+}, and Pb^{2+} adsorptions were heterogeneous, spontaneous, endothermic, and irreversible processes. The adsorptions of Cu^{2+} and Cd^{2+} were dominated by physisorption, while the chemisorption was dominant in Pb^{2+} adsorption. The results of column experiments suggested that the B-Al/Mg had the potential application in purification of drinking water in practice because its removal for Cu^{2+}, Cd^{2+}, and Pb^{2+} was greater than activated carbons selected in this study, and the breakthrough times were up to 20–30 d. The dynamic adsorptions of Cu^{2+}, Cd^{2+}, and Pb^{2+} were well described by BDST model. B-Al/Mg had the potential for commercial applications. For single heavy metal removal, the advised adsorption columns were column 4 (Cu^{2+} and Pb^{2+}) and column 1 (Cd^{2+}). And the column 5 was suggested for Cu^{2+}, Cd^{2+}, and Pb^{2+} competitive adsorption.

Acknowledgement

This work was supported by the Programs of National Natural Science of China (51608143, 51638006), Guangxi science and technology program (Guike AD17195023), Program for High Level Innovation Team and Outstanding Scholar of Universities in Guangxi (Gui Cai Jiao Han [2018] 319), Guangxi young and middle-aged teachers basic ability promotion project (2017KY0244), Guangxi special experts funded projects (Beidou Xi) and Special funding for Guangxi 'BaGui Scholar'construction projects(Huijuan Liu).

References

[1] W.Q. Zhu, W.H. Du, X.Y. Shen, H.J. Zhang, Y. Ding, Comparative adsorption of Pb^{2+} and Cd^{2+} by cow manure and its vermicompost, Environ. Pollut., 227 (2017) 89–97.
[2] M.M.U.R. Khattak, M. Zahoor, B. Muhammad, F.A. Khan, R. Ullah, N.M. AbdEI-Salam, J. Nanomate., Removal of heavy metals from drinking water by magnetic carbon nanostructures prepared from biomass, J. Nanomater., 2017 (2017) 5670371.
[3] E. Kokkinos, K. Simeonidis, A. Zouboulis, M. Mitrakas, Mercury removal from drinking water by single iron and binary iron-manganese oxyhydroxides, Desal. Wat. Treat., 54 (2015) 2082–2090.
[4] A. Petrovič, M. Simonič, Removal of heavy metal ions from drinking water by alginate-immobilised Chlorella sorokiniana, Int. J. Environ. Sci. Technol., 13 (2016) 1761–1780.
[5] G. Iervolino, V. Vaiano, L. Rizzo, G. Sarno, A. Farinaa, D. Sannino, Removal of arsenic from drinking water by photocatalytic oxidation on $MoOx/TiO_2$ and adsorption on γ-Al_2O_3, J. Chem. Technol. Biotechnol., 91 (2016) 88–95.
[6] A. Jones, W.R. Knocke, Evaluating the role of soluble aluminum in manganese removal via MnOx(s)-coated filtration media in drinking water treatment, Water Res., 111 (2017) 59–65.
[7] M.F. Zhu, L. Zhu, J.L. Wang, T.L. Yue, R.H. Li, Z.H. Li, Adsorption of Cd(II) and Pb(II) by in situ oxidized Fe3O4 membrane grafted on 316L porous stainless steel filter tube and its potential application for drinking water treatment, J. Environ. Manage., 196 (2017) 127–136.
[8] B.B. Li, F. Zhou, K. Huang, Y.P. Wang, S.R. Mei, Y.K. Zhou, T. Jing, Environmentally friendly chitosan/PEI-grafted magnetic gelatin for the highly effective removal of heavy metals from drinking water, Sci. Rep. UK, 7 (2017) 43082.
[9] S. Lung, H.H. Li, S.C. Bondy, A. Campbell, Low concentrations of copper in drinking water increase AP-1 binding in the brain, Toxicol. Ind. Health, 31 (2015) 1178–1184.
[10] S.A. Moreira, D.Q. Melo, A.C.A.D. Lima, F.W. Sousa, A.G. Oliveira, A.H.B. Oliveira, R.F. Nascimento, Removal of Ni^{2+}, Cu^{2+}, Zn^{2+}, Cd^{2+} and Pb^{2+} ions from aqueous solutions using cashew peduncle bagasse as an eco-friendly biosorbent, Desal. Wat. Treat., 57 (2016) 10462–10475.
[11] M. Nemati, S.M. Hosseini, M. Shabanian, Novel electrodialysis cation exchange membrane prepared by 2-acrylamido-2-methylpropane sulfonic acid; heavy metal ions removal, J. Hazard. Mater., 337 (2017) 90–104.
[12] R. Ahmad, I. Hasan, L-cystein modified bentonite-cellulose nanocomposite (cellu/cys-bent) for adsorption of Cu^{2+}, Pb^{2+}, and Cd^{2+} ions from aqueous solution, Sep. Sci. Technol., 51 (2016) 381–394.
[13] L.G. Yan, S. Li, H.Q. Yu, R.R. Shan, B. Du, T.T. Liu, Facile solvothermal synthesis of Fe3O4/bentonite for efficient removal of heavy metals from aqueous solution, Powder Technol., 301 (2016) 632–640.
[14] X.H. Liu, C. Cheng, C.J. Xiao, D.D. Shao, Z.M. Xu, J.Q. Wang, S.H. Hu, X.L. Li, W.J. Wang, Polyaniline (PANI) modified bentonite by plasma technique for U(VI) removal from aqueous solution, Appl. Surf. Sci., 411 (2017) 331–337.
[15] X.Y. Jin, M. Zheng, B. Sarkar, R. Naidu, Z.L. Chen, Characterization of bentonite modified with humic acid for the removal of Cu (II) and 2,4-dichlorophenol from aqueous solution, Appl. Clay Sci., 134 (2016) 89–94.
[16] K. Al-Essa, Activation of Jordanian Bentonite by hydrochloric acid and its potential for olive mill wastewater enhanced treatment, J. Chem., 2018 (2018) 8385692.

[17] T. Şahan, F. Erol, Ş. Yılmaz, Mercury(II) adsorption by a novel adsorbent mercapto-modified bentonite using ICP-OES and use of response surface methodology for optimization, Microchem. J., 138 (2018) 360–368.
[18] T. Schütz, S. Dolinská, P. Hudec, A. Mockovčiaková, I. Znamenáčková, Cadmium adsorption on manganese modified bentonite and bentonite-quartz sand blend, Int. J. Miner. Process., 150 (2016) 32–38.
[19] B. Sadeghalvad, H.S. Karimi, H. Hosseinzadegan, A.R. Azadmehr, A comparative study on the removal of lead from industrial wastewater by adsorption onto raw and modified Iranian bentonite (from Isfahan area), Desal. Wat. Treat., 52 (2014) 6440–6452.
[20] Ö. Şahin, M. Kaya, C. Saka, Plasma-surface modification on bentonite clay to improve the performance of adsorption of methylene blue, Appl. Clay Sci., S116/117 (2015) 46–53.
[21] B. Benli, Effect of borax addition on the structural modification of bentonite in biodegradable alginate-based biocomposites, J. Appl. Polym. Sci., 128 (2013) 4172–4180.
[22] A. Fehervari, W.P. Gates, T.W. Turney, A.F. Patti, A. Bouazza, Cyclic organic carbonate modification of sodium bentonite for enhanced containment of hyper saline leachates, Appl. Clay Sci., 134 (2016) 2–12.
[23] C.F. Shi, X.C. Guo, M.J. Jiang, Y. He, Study on the effect of surface modification on the properties of bentonite greases, Chin. Petrol. Process. Petrochem. Technol., 18 (2016) 99–109.
[24] L.H. Liu, Y. Lin, Y.Y. Liu, H. Zhu, Q. He, Removal of methylene blue from aqueous solutions by sewage sludge based granular activated carbon: adsorption equilibrium, kinetics, and thermodynamics, J. Chem. Eng. Data, 58 (2013) 2248–2253.
[25] A. Javaid, R. Bajwa, U. Shafique, J. Anwar, Removal of heavy metals by adsorption on Pleurotus ostreatus, Biomass Bioenergy, 35 (2011) 1675–1682.
[26] B. Anna, M. Kleopas, S. Constantine, F. Anestis, B. Maria, Adsorption of Cd(II), Cu(II), Ni(II) and Pb(II) onto natural bentonite: study in mono- and multi-metal systems, Environ. Earth Sci., 73 (2015) 5435–5444.
[27] J.H. Yan, G.H. Lan, H.Y. Qiu, C. Chen, Y.Q. Liu, G.Y. Du, J.H. Zhang, Adsorption of heavy metals and methylene blue from aqueous solution with citric acid modified peach stone, Sep. Sci. Technol., 53 (2018) 1678–1688.
[28] M.E. Bouraie, A.A. Masoud, Adsorption of phosphate ions from aqueous solution by modified bentonite with magnesium hydroxide $Mg(OH)_2$, Appl. Clay Sci., 140 (2017) 157–164.
[29] L.H. Liu, H. Lin, F. Pan, G. Wang, D.Q. Wang, Modification of activated carbons by HNO_3 and H_2O_2 for removal of methylene blue dye from aqueous solutions, Desal. Wat. Treat., 114 (2018) 297–306.
[30] M. Nainamalai, M. Palani, B. Soundarajan, E.J.S.S. Allwin, Decolorization of synthetic dye wastewater using packed bed electro-adsorption column, Chem. Eng. Process., 130 (2018) 160–168.
[31] L.H. Xu, S.D. Wang, J.W. Zhou, H.H. Deng, R.L. Frost, Column adsorption of 2-naphthol from aqueous solution using carbon nanotube-based composite adsorbent, Chem. Eng. J., 335 (2018) 450–457.